BUDAPEST UNIVERSITY OF TECHNOLOGY AND ECONOMICS
FACULTY OF ARCHITECTURE
DEPARTMENT OF MECHANICS, MATERIALS AND STRUCTURES

SAND IN HAND

HEGYMEGI JULIA
ADVISORS: PROF. GÁBOR DOMOKOS, ESZTER FEHÉR
RESEARCH PAPER_TDK 2017

CONTENT

1. Introduction

During the summer of 2017 I have spent two months in the UK, working in a children's holiday camp. This was not just my first time being abroad for a longer period of time, but also my first time getting closer to nature on a scientific basis. Whenever I wanted to escape the hustle of town I went North to experience the calmness of the Salfleetby Theddlethorpe National Nature Reserve (fig. 1.). I was hoping, that I could find out more about the story of the inanimate world. Observing the sand on the shore was a new, and unique experience for me.

Fig. 1. Sampling location: Saltfleetby Theddlethorpe National Nature Reserve, England

1.1 Sampling

Lot of field studies on natural shapes have been carried out. For instance, in a gypsum field in New Mexico, abrasion and sorting of sand were measured quantitively [1]. Although in our case the material of the sand was much harder (quartz), we still first hoped to find correlation between the spatial location of the sampling points and the morphology of the grains. As we will describe, the truth turned out to be different, although even more interesting. My sampling area, the Salfleetby Theddlethorpe National Nature Reserve consists of several rare habitats shaped by the sea, the tides and the wind. The sand was collected from 13 different locations along a perpendicular line to the coast (fig. 1.1). This sampling line was approximately 120 metres long with 3 different types of landmarks; 1 – sandy area from mid tide line, 2 – bushy area with smaller dune forms, 3 – bigger dunes running from North to South. Through the sandy part I chose the sampling locations evenly in distance. Once hitting the

dunes, the samples were collected from the dune crests in order not to mix the sea to land pattern with an over a dune pattern.

Fig. 1.1. Prependicular sampling line to the shore, along which the 13 samples were collected

1.2. Observation

These samples were taken back to Hungary and analysed individually in the laboratory of the Department of Mechanics, Materials and Structures at the University of Technology and Economics in Budapest.

1. First photos of the grains were taken with a camera attached to a microscope (fig. 1.2),
2. With a MATLAB software provided by the Department geometric data from their contours were obtained.

Fig.1.2. Taking pictures of the grains with a camera attached to a microscope in the Laboratory of the Department of Mechanics, Materials and Structure, Budapest

These geometric data included surface area (*A*), convexity (*C*), isoperimetric ratio (*I*) and axis ratio (*R*).

1. Area (*A*)
   The amount of space inside the boundary of a 2-dimensional shape

2. Convexity (*C*)
   $C=(A_c-A)/A$
   where A_c stands for the area of the convex outline of the shape and *A* is the area of the shape.

3. Isoperimetric ratio (*I*)
   $I=4\pi A/p^2$,
   where *A* is the area, and *p* the perimeter of the shape.
   We observe that for all shapes $0<I\leq 1$ and $I=1$ is only obtained for the circle.

4. Axis ratio *(R)*
   $R=e/f$
   the shorter axis (*e*), divided by the longer axis (*f*) of the shape.
   We define the longer axis as the maximal diameter and the shorter axis as the diameter orthogonal to the longer axis. We also observe that for all shapes $0<R\leq 1$.

Each of the sampling locations had between 40-50 successfully processed grain data, from which I counted the mean value and the standard deviation for each of the sampling locations.

During the evaluation of the data, what made us curious is that the mean value of *I* and *R* almost equalled to each other through all the sampling locations. The main goal of my research is to explore this phenomenon with mathematical and geomorphological tools.

2. Field data

The mean values and standard deviations of *A,C,I,R* can be seen in Figure 2.1. Fig. 2.2, represents these data in a form of a diagram. One can realize how close the mean values of *I* and *R* are to each other.

It is even more spectacular in Figure 2.3 where the two axes are *R* and *I*. We may observe that for all measurements $0.74 < I,R < 0.78$, all the data points lie within square with area less than 0.2% of the area of the unit square. Through the rest of my research I would like to prove that this may not be a pure coincidence, in fact, I will argue that a plausible mathematical model provides a surprising, yet appealing explanation for this phenomenon.

Sampling location	*I*		*C*		*R*		*A*	
	mean value	st. deviation	mean value	st. deviation	mean value	st. deviation	mean value	st. deviation
D1	0,740	0,059	0,950	0,015	0,772	0,134	91785,306	29216,407
D2	0,767	0,042	0,956	0,016	0,782	0,104	72631,962	25469,328
D3	0,763	0,046	0,956	0,014	0,786	0,116	63168,129	23831,468
D4	0,747	0,052	0,946	0,018	0,770	0,096	62745,717	21516,089
D5	0,765	0,046	0,956	0,016	0,758	0,103	65236,797	20525,032
B1	0,751	0,043	0,951	0,016	0,745	0,102	72064,850	27155,854
B2	0,752	0,050	0,954	0,016	0,760	0,131	78822,345	26455,373
B3	0,751	0,043	0,950	0,018	0,769	0,104	75054,537	21031,672
B4	0,759	0,045	0,954	0,012	0,779	0,104	67581,756	26091,709
H1	0,770	0,055	0,957	0,017	0,796	0,118	69003,160	17996,672
H2	0,774	0,053	0,961	0,015	0,770	0,102	73904,490	26021,290
H3	0,772	0,054	0,955	0,024	0,769	0,095	82216,591	37137,316
H4	0,772	0,044	0,960	0,012	0,777	0,117	65834,987	27258,661

Fig. 2.1 Table of the mean values and standard deviations of *I,C,R,A* belonging to the different sampling locations.

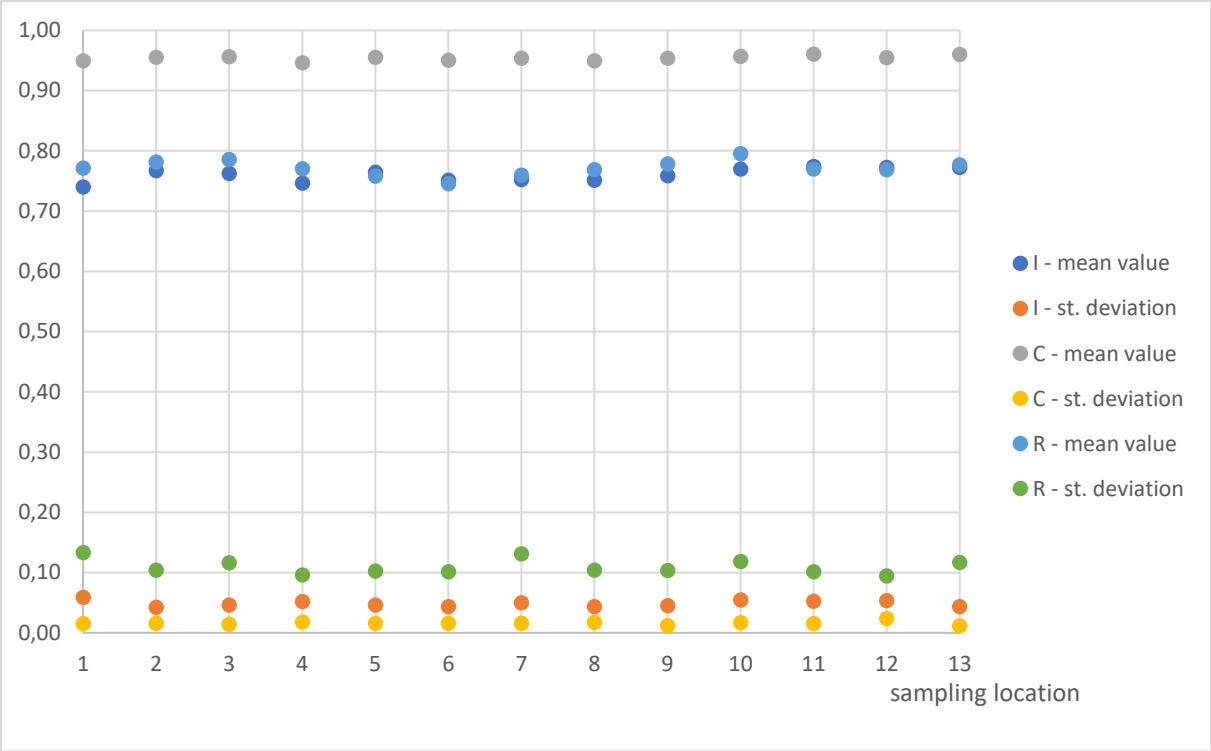

Fig. 2.2 Diagram of the mean values and standard deviations of *I,C,R* belonging to the 13 different sampling locations.

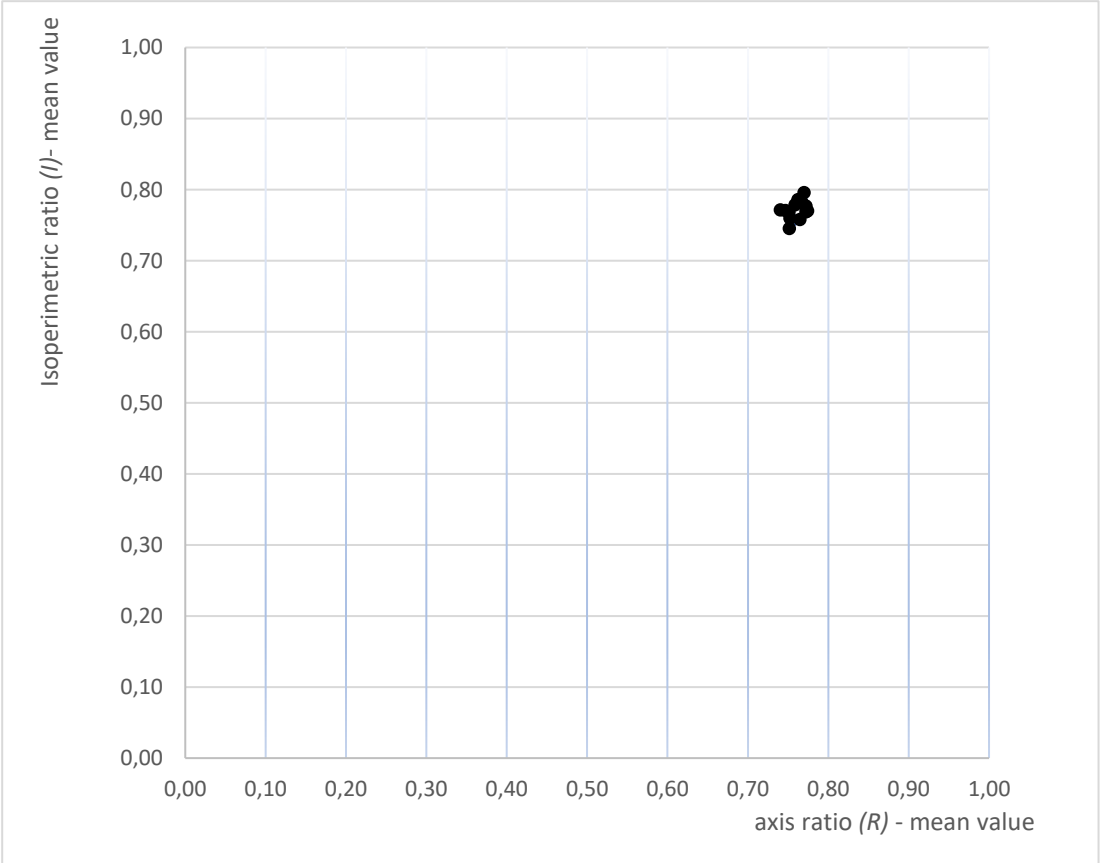

Fig.2.3 Diagram of the mean values of *R* and *I*, emphasizing the small range (0,74-0,78) within it values.

3. Mathematical modelling

3.1. The co- evolution of *I* and *R* under orthogonal affinity

To explain the coincidence of the two variables *I* and *R* it appeared to be a natural idea to study one parameter families of shapes.

For simplifying the case, I have examined the evolution $I(\lambda)$ and $R(\lambda)$ in case of a twice (D_2) symmetric convex shape *S*, being transformed under linear affinity with parameter λ, parallel to one of the symmetry axes . Conveniently, we can set $\lambda=1$ for $R=1$. Using this convenient scaling we can see immediately that for any choice of *S*, the evolution $R(\lambda)$ will be identical:

(1) if $\lambda<1$ then $R(\lambda)=\lambda$, otherwise $R(\lambda)=1/\lambda$

while the affine evolution of different shapes implies, in general, different evolutions $I(\lambda)$. Below, on diagram 3.1 we can see this general $R(\lambda)$ function given in equation (1) and the $I(\lambda)$ functions in case of a rhombus and a rectangle.

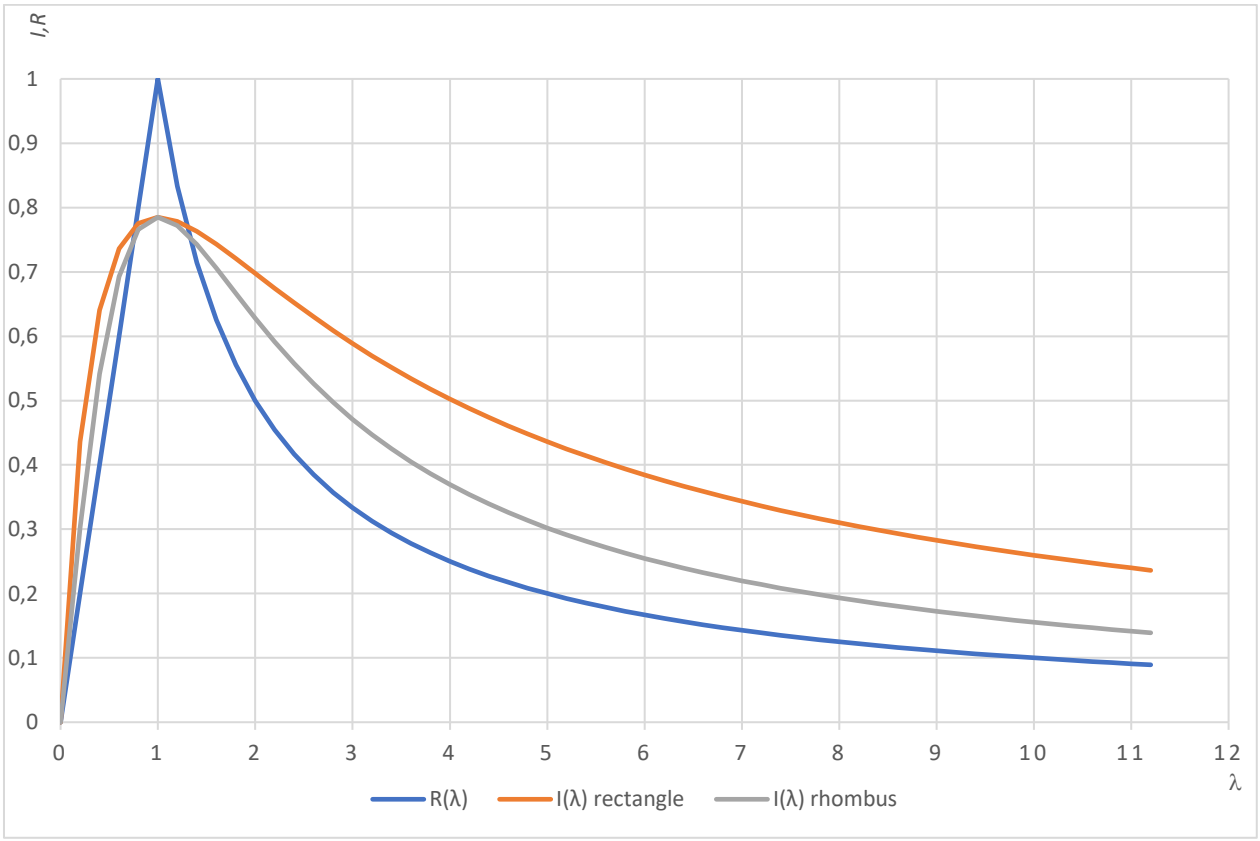

Fig. 3.1 Diagram of $R(\lambda)$, $I(\lambda)_{rhombus}$, and $I(\lambda)_{rectangle}$

We are interested in the values for the intersection points of *I(λ)* and *R(λ)*, and whether such intersection exists for all geometric shape families.

The intersection points *R(λ)=I(λ)* can be computed easily for the rhombus, the rectangle and the ellipse:

Computation of intersection points */I(λ)=R(λ)/*

1. Ellipse – Circle

$$I = \frac{d}{d} = 1$$

$$R = \frac{4\pi r^2 \pi}{(2r\pi)^2} = 1$$

2. Rectangle

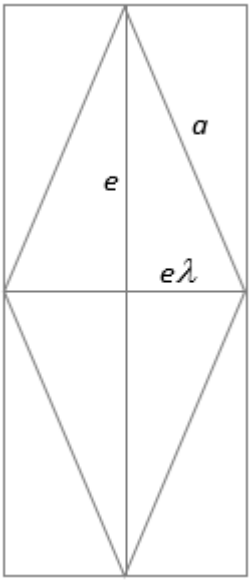

0≤λ≤1

$$4\pi \frac{4e^2\,\lambda}{(4e + 4e\lambda)^2} = \frac{e\lambda}{e}$$

$$\frac{16\pi e^2 \lambda}{16e^2(1 + 2\lambda + \lambda^2)} = \lambda$$

$$0 = \lambda^2 + 2\lambda + 1 - \pi$$

λ_1=0,7724

(λ_2=-0,2275)

1≤λ

$$4\pi \frac{4e^2\,\lambda}{(4e + 4e\lambda)^2} = \frac{e}{e\lambda}$$

$$\frac{16\pi e^2 \lambda}{16e^2(1 + 2\lambda + \lambda^2)} = \frac{1}{\lambda}$$

$$0 = (\pi - 1)\lambda^2 - 2\lambda - 1$$

$\underline{\lambda_3 = 1{,}2946 = 1/\lambda_1}$

(λ_4=-0,3607)

3. Rhombus

$0 \leq \lambda \leq 1$

$$4\pi \frac{2e^2\,\lambda}{(4a)^2} = \frac{e\lambda}{e}$$

$$\frac{8\pi e^2 \lambda}{8e^2(2\lambda^2 + 2)} = \lambda$$

$$0 = 2\lambda^2 + 2 - \pi$$

$\underline{\lambda_1 = 0{,}7555}$

(λ_2=-0,7555)

$1 \leq \lambda$

$$4\pi \frac{2e^2\,\lambda}{(4a)^2} = \frac{e}{e\lambda}$$

$$\frac{8\pi e^2 \lambda}{8e^2(2\lambda^2 + 2)} = \frac{1}{\lambda}$$

$$0 = (\pi - 2)\lambda^2 - 2$$

$\underline{\lambda_3 = 1{,}3236 = 1/\lambda_1}$

(λ_4=-13,236)

The above simple computations suggest that such intersection points may exist for arbitrary choice of *S.* In particular, we propose the following

Theorem 1: For an arbitrary convex curve *S* with D_2-symmetry, the one parameter family $S(\lambda)$ generated by orthogonal affinity in the direction of one of the symmetry axes will always contain two shapes $S(\lambda_1)$, $S(\lambda_2)$ with $\lambda_1 \leq \lambda_2$ such that here $R(\lambda_i)=I(\lambda_i)$ and $\lambda_1=\lambda_2$ holds only if *S* is an ellipse.

Proof of Theorem 1:

First we make the following

Remark 1:

$$\exists \lambda: I(\lambda) < R(\lambda)$$

The maximum value of both functions is 1. We know that *I* reaches 1 only in case of a circle. As circle is an ideal form, and in Nature shapes can never reach the state of being perfect circles, we know for sure that *I* will never value 1.

In order to prove the presence of intersection points we have to prove the opposite side as well:

Lemma 1:

In case of an arbitary twice symmetric convex shape (*S*), being transformed under linear affinity with parameter λ parallel to one of the symmetry axes, there exists a value of λ, where $I(\lambda)>R(\lambda)$.

Proof of Lemma 1:

We start with

Remark 2:

(a) At a fixed axis ratio *S* has its lower extreme of perimeter and area when *S* is a rhombus.

(b) At a fixed axis ratio *S* has its upper extreme of perimeter and area when *S* is a rectangle.

The squared perimeter (p^2) and area (A) of an arbitrary rhombus and of an arbitrary rectangle:

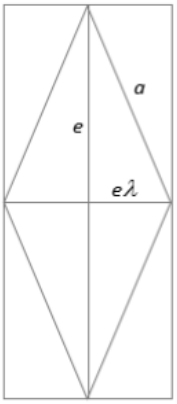

	rhombus (min)	rectangle (max)
p^2	$(4a)^2=16(e^2\lambda^2+e^2)$	$(4e+4e\lambda)^2=16(e^2+e^2\lambda^2+2e^2\lambda)$
A	$2e*\lambda e=2e^2\lambda$	$4e*4e\lambda=4e^2\lambda$

We set the half of the axis that is perpendicular to the direction of the affinity to 1. *(e=1)*

We have 2 possibilities:

If $0 \leq \lambda \leq 1$

$$\frac{4\pi A}{p^2} > \frac{1\lambda}{1}$$

If $\lambda \geq 1$

$$4\pi \frac{A}{p^2} > \frac{1}{\lambda}$$

case 1. $0 \leq \lambda \leq 1$

Remark 3: Let *x* and *y* be two variable quantities. If $d < \frac{x(min)}{y(max)}$ stands, then $d < \frac{x}{y}$ for all values of *x* and *y*.

Based on Remarks 2 and 3, we can insert the data of the rhombus as the minima for *A*, and the data of the rectangle as the maxima for p^2

$$\lambda < \frac{4\pi * 2\lambda}{16(1+\lambda^2+2\lambda)}$$

$$16(1+\lambda^2+2\lambda) < 8\pi$$

$$2\lambda^2 + 4\lambda + 2 - \pi < 0$$

$$\lambda = \frac{-4 \pm \sqrt{4^2 - 4 * 2 * (2 - \pi)}}{4}$$

λ_1=0,2533

(λ_2=-2,2533)

D≥0, and 0≤λ_1≤1, meaning there exists a value of λ where the inequality is true.

case 2. $\lambda \geq 1$

$\frac{1}{\lambda} < \frac{x}{y}$ → $0 < \frac{1}{\lambda} \leq 1$, the worst possibility is the same as in case 1.

$$\frac{1}{\lambda} < \frac{4\pi * 2\lambda}{16(1 + \lambda^2 + 2\lambda)}$$

$$2\lambda^2 + 4\lambda + 2 < \pi\lambda^2$$

$$(2 - \pi)\lambda^2 + 4\lambda + 2 < 0$$

$$\lambda = \frac{-4 \pm \sqrt{4^2 - 4(2 - \pi)2}}{2(2 - \pi)}$$

λ_1=3,9477

(λ_2=-0,4438)

D≥0, and 0≤λ_1≤1, meaning there exists a value of λ, where the inequality is true.

Q.e.d.

Theorem 1 reveals that each family *S(λ)* must carry this special ratio and this ratio would be characteristic of that particular family, so by knowing the λ_i values belonging to $I(\lambda)=a(\lambda)$, we may be able to draw conclusions for a shape. In particular, the observed λ_i values in case of the measured sand are in close vicinity for the values computed for the rectangle and the rhombus, so this suggests that grain contours may look like slightly elongated rectangles. In fact, at closer

inspection this appears to be the case: most of them can be well approximated by these slightly elongated rectangles (cf. Figure 3.2.4).

3.2 Fragmentation model

Fragmentation models might provide a possible answer for the history of shapes since they represent the initial conditions for the evolution equations. There are general results about the universal correspondence between size and elongation of fragments [2]. Here our goal is somewhat similar: we aim to describe some universal geometric features characterizing 2D fragmentation.

A simplified, planar fragmentation model operating by splitting convex polygons into two parts by random straight lines shows that, regardless of the initial shape, after sufficiently many fragmentation events the average value of vertices (and edges) approaches 4. One may, based on this simple model say that natural (planar) fragments tend to be quadrangles.

We can formalize our model as follows. Among a set of convex polygons *S*, let *d* denote the number of polygons and *n* denote the total number of vertices. Arbitrarily we choose one convex polygon from the set and split it into two parts with an arbitrary straight line. Then we put the newly obtained two polygons back in the set. *t* denotes the number, how many times this operation has been applied. Now we formulate

Theorem 2:

$$\lim_{t\to\infty} \frac{n(t)}{d(t)} = 4$$

Proof of Theorem 2:

We prove this statement by a simple topological observation. If a convex polygon is intersected by a straight line then there are always two intersection points and in a generic case none of these will coincide with a vertex of the original polygon. Since both intersection points will be

vertices of both new polygons this implies that in each splitting event the number of total vertices is increased by 4 and the number of polygons is increased by 1. So after *s* splitting events we will have *s+1* polygons with *n+4s* vertices, where *n* is the number of vertices of the initial polygon. Clearly, as *s* tends to infinity, the ratio *(n+4s)/(1+s)* approaches 4. This argument proves Theorem 2.

Q.e.d.

Remark 4

Not only the average of vertices will approach 4, but the obtained convex polygons will tend to be quadrangles as well, meaning the standard deviation of the number of vertices will be in close vicinity to 0. If *n>4* the convex polygon has a higher probability of decreasing its number of vertices than increasing them. These convex *n-gons* where *n>4* are quite unstable, and the presence of them will be negligible after many successful fragmentation events.

Thus, this simplified, planar fragmentation model is able to explain through a geomorphological process the quadrangles seen in the contours. (fig. 3.2.4)

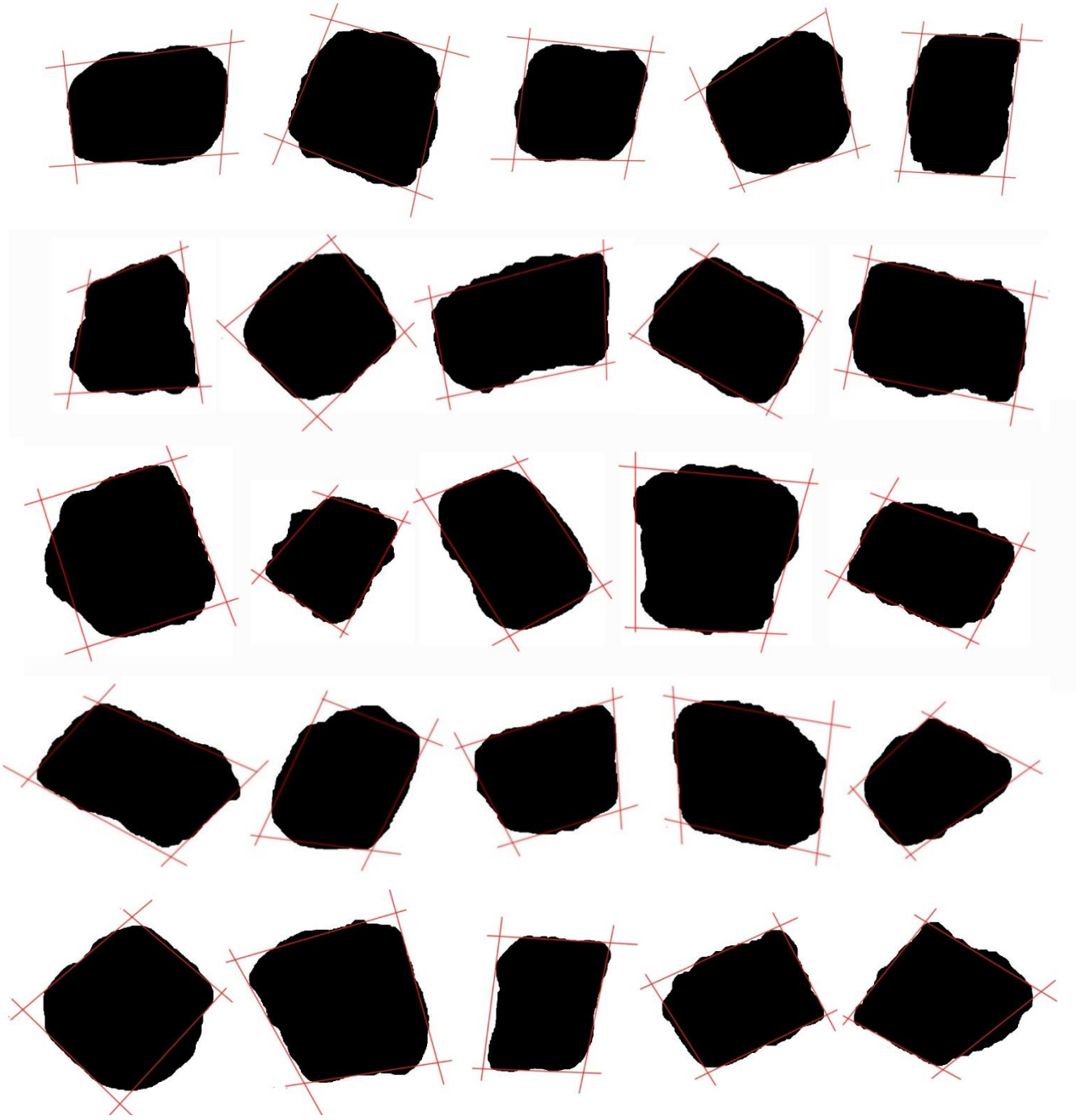

Fig. 3.2.4 Some contours of the grains, depicting the slightly elongated rectangles with which, they can be approximated

.

4. Conclusions

All in all, the sand samples that I collected from the astonishing shore of England seem to reveal much more by the geometric data coded in them than I first expected they would. I photographed the grains of sand with the help of a camera attached to a microscope and analysed their contours in a MATLAB programme. Most of the processed grain photos could be approximated with slightly elongated rectangles. In the research, I came up with two mathematical models, which provide appealing explanations for this phenomenon.

Firstly, the mean value for both *I* and *R* through the 13 locations varied within the range of 0,74-0,78. Theorem 1 proved that, to each one-parameter (λ), D_2-symmetric family $S(\lambda)$ of convex shapes there exists two critical parameter values $\lambda_1 \leq \lambda_2$ such that $R(\lambda_i)=I(\lambda_i)$. The lower critical λ_i computed for the rectangle is 0,7724, for the rhombus 0,7555 which are remarkably close to the λ values for the measured sand. Since the rectangle and the rhombus are the only admissible quadrangles in this model this suggests that the contours may indeed be close to quadrangles.

Beyond the co-evolution of *I* and *R*, there exists a completely independent argument supporting that fragmented grains should have contours close to quadrangles. This argument relies on a simplified geometric fragmentation model and in Theorem 2 it is shown by a purely topological method that after sufficiently many successful fragmentation events of splitting 2D convex polygons into two by random straight lines, the average number of the edges will be arbitrarily close to 4.

Both independent theoretical arguments suggest that fragment contours may be well approximated by slightly elongated quadrangles. By looking at the images I found that this is indeed the case (cf. Fig 3.2.4.). This observation not only suggests that there may be indeed a relation between these mathematical models and the behaviour of Nature experienced on the coast but also offers a beautiful example where field work and mathematical reasoning go hand in sand.

5. Acknowledgements

I would like to thank Professor Gábor Domokos for his guidance through the whole research, and Eszter Fehér for providing support in analysing the samples.

6. Appendix

1. A special case of the fragmentation model explained before. Examining the evolution of one convex polygon.

   Let $n(P)$ denote the number of vertices of a convex P. By intersecting the polygon P_0 with a straight line we split it into two convex polygons $P_{1,1}$ and $P_{1,2}$ and we apply this operation consecutively k times to every such obtained polygon to obtain 2^k polygons $P_{k,j}$ ($j=1,2, \ldots 2^k$). Now we formulate

$$\lim_{k\to\infty} \frac{\sum_{j=1}^{2^k} n(P_{k,j})}{2^k} = 4$$

2. Figures indicating the way the simplified fragmentation operates

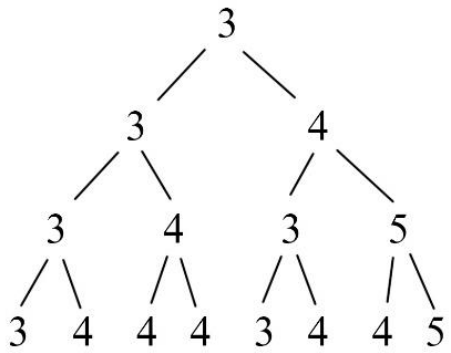

Fig. 5.2.1 An evolution of a triangle highlighting the number of vertices through 3 random sufficient

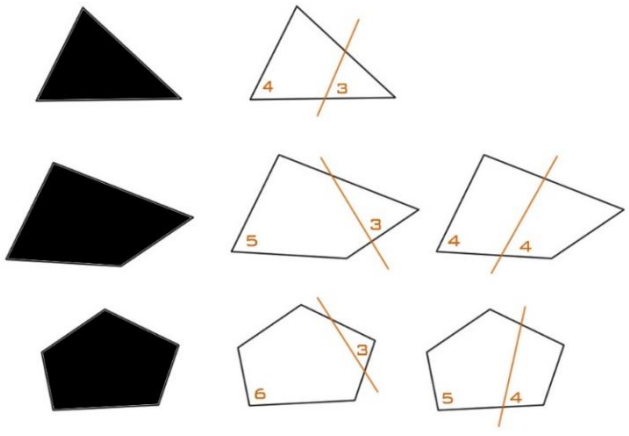

Fig. 5.2.2 A figure indicating the possible results of the simplified planar fragmentation model in case of a triangle, a rectangle and a pentagon.

.

3. The direct photos of grains recorded by the camera and sent to the pc. The grains have been photographed in a 2*2mm square in order to count their areas.

4. Sketches made and used during field work

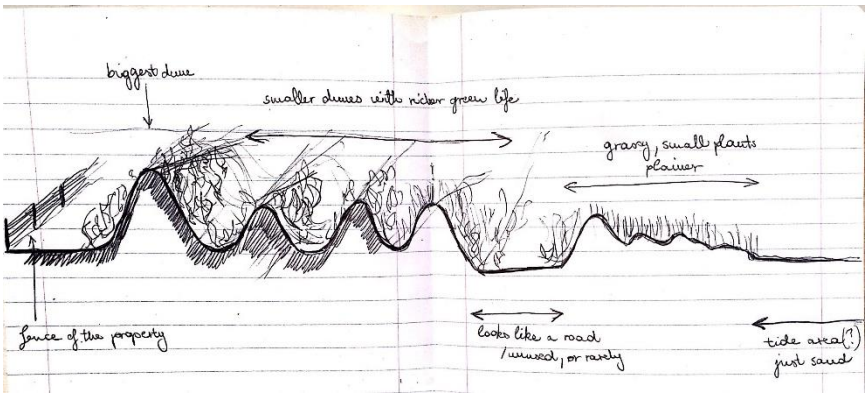

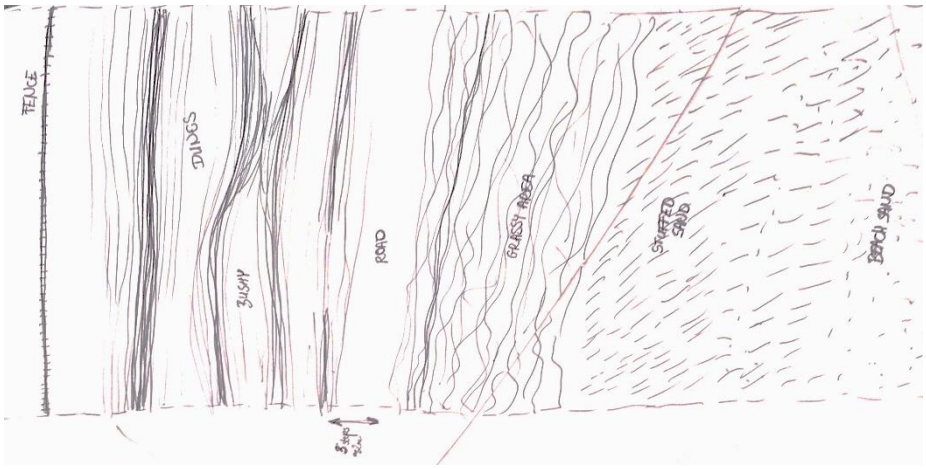

5. Further photos of sampling at Saltfleetby Theddlethorpe Natural Reserve

7. References

[1.] Douglas J. Jerolmack, Meredith D. Reitz, Raleigh L. Martin, *Sorting out abrasion in a gypsum dune field,* Journal of Geographical Research: Earth Surface (2011), DOI: 10.1029/210JF001821

[2.] Gábor Domokos, Ferenc Kun, András Árpád Sipos, Tímea Szabó, *Universality of fragment shapes*, Scientific Reports **5** (2015), DOI: 10.1038/srep09147